Mixed basin boundary structures of chaotic systems

Epaminondas Rosa, Jr.* and Edward Ott†
Institute for Plasma Research, University of Maryland, College Park, Maryland 20742
(Received 13 July 1998)

Motivated by recent numerical observations on a four-dimensional continuous-time dynamical system, we consider different types of basin boundary structures for chaotic systems. These general structures are essentially mixtures of the previously known types of basin boundaries where the character of the boundary assumes features of the previously known boundary types at different points arbitrarily finely interspersed in the boundary. For example, we discuss situations where an everywhere continuous boundary that is otherwise smooth and differentiable at almost every point has an embedded uncountable, zero Lebesgue measure set of points at which the boundary curve is nondifferentiable. Although the nondifferentiable set is only of zero Lebesgue measure, the curve's fractal dimension may (depending on parameters) still be greater than one. In addition, we discuss bifurcations from such a mixed boundary to a ''pure'' boundary that is a fractal nowhere differentiable curve or surface and to a pure nonfractal boundary that is everywhere smooth.
[S1063-651X(99)02401-0]

PACS number(s): 05.45.Gg

I. INTRODUCTION

The coexistence of two or more attractors provides for different long-time behaviors of a dynamical system depending on its initial conditions. The set of points that asymptotically approach a given attractor (its basin of attraction) will have a boundary with the basin of attraction of the other attractor or attractors. Knowledge of the basin and its boundary thus supplies important information allowing a prediction of the long-term behavior of a system. Basin boundaries can be either smooth or fractal and have been extensively studied [1–6]. This paper is motivated by a recent study in which we observed a basin boundary structure that we believe has previously not been seen or noted [7]. Our previous study involved a four-dimensional flow. This presented difficulties for computational analysis and verification of the suspected boundary structure. For this reason, in this paper we restrict most of our discussion to the case of simple maps, where understanding and computational verification are readily available. We begin by reviewing some relevant background material.

A. Background

For typical dynamical systems, three basic characteristic topologies [1–6] of basin boundaries have been found [8].

(a) The basin boundary can be a smooth curve or surface. An example of this [9] is shown in Fig. 1(a) for the Hénon map

$$x_{n+1}=A-x_n^2-Jy_n, \tag{1a}$$

$$y_{n+1}=x_n, \tag{1b}$$

with $A=1.150$ and $J=0.3$. For these parameter values there are two attractors giving the long-term behavior of the system for almost all initial conditions; the attractor for points in the black basin shown in Fig. 1(a) is $(x,y)\to\infty$, while the attractor for points in the blank basin is a periodic orbit of period 1.

(b) The boundary can locally have the character of a Cantor set of smooth curves or surfaces. This is illustrated [9] in Fig. 1(b) and the blowup in Fig. 1(c) for the Hénon map with parameters $A=1.405$ and $J=0.3$. (In this case the attractor corresponding to the blank region is a periodic orbit of period 2.)

(c) The boundary can be a continuous nowhere differentiable curve or surface. A simple example of this is provided by the map [1,2]

$$y_{n+1}=\lambda_y y_n+\cos(2\pi x_n), \tag{2a}$$

$$x_{n+1}=\lambda_x x_n \bmod 1, \tag{2b}$$

with λ_x and λ_y greater than 1 and λ_x an integer greater than λ_y. This map has no attractor with finite y and almost all initial conditions generate orbits that approach either $y=+\infty$ or $y=-\infty$, which we regard as the two attractors for the system. Figure 1(d) shows the basin structure for this system with $\lambda_x=3$ and $\lambda_y=1.5$. Blank corresponds to the basin of $y=+\infty$ and black to the basin of $y=-\infty$. In this case one can analytically derive the equation of the basin boundary [1,2]

$$y=-\sum_{j=1}^{\infty}\lambda_y^{-j}\cos(2\pi\lambda_x^{j-1}x)=f_W(x). \tag{3}$$

The function $f_W(x)$ is continuous and for $\lambda_y<\lambda_x$ is nowhere differentiable (a Weierstrass curve) and fractal with dimension

$$d=2-\ln\lambda_y/\ln\lambda_x. \tag{4}$$

*Present address: Nonlinear Dynamics Laboratory, Department of Physics, University of Miami, Coral Gables, FL 33146. Electronic address: epa@physics.miami.edu

†Also at Department of Physics, Department of Electrical Engineering, and Institute for Systems Research, University of Maryland, College Park, MD 20742.

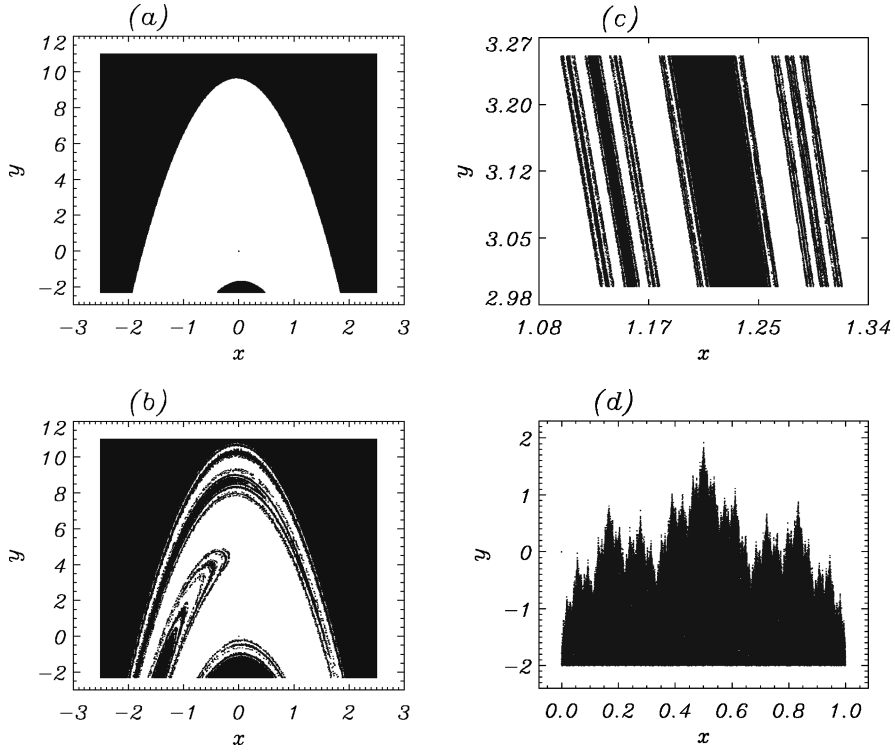

FIG. 1. (a) Smooth basin boundary for the Hénon map. (b) Fractal basin boundary for the Hénon map. (c) Enlargement of (b). (d) Basin boundary that is a continuous nowhere differentiable curve.

For $\lambda_y > \lambda_x$, on the other hand, $f_W(x)$ is everywhere differentiable and consequently has dimension one (nonfractal).

For typical dynamical systems represented by two-dimensional invertible maps and three-dimensional flows, boundary types *a* and *b* and mixtures thereof [10] appear to be the only types of basin boundaries. Boundary type *c* is possible for higher-dimensional invertible maps (map dimensionality $\geqslant 3$) or flows (dimensionality $\geqslant 4$) or for two-dimensional noninvertible maps [e.g., Eqs. (2)].

Although basin types *b* and *c* are both fractal, they are fundamentally different. One aspect of this difference is provided by the concept of accessibility [3]. We say a point *x* on a basin boundary is *accessible* from a given basin *B* if it is possible to draw a finite length curve connecting a point in the interior of *B* to *x* such that the curve never crosses a basin boundary. Clearly, this is the case for a boundary of type *a*. It is also the case for a boundary of type *c*. [For example, for the case of Eq. (3), any point on the boundary (x_b, y_b), where $y_b = f_W(x_b)$, is accessible from a point $(x_b, y_b + \Delta)$ with $\Delta > 0$ $(\Delta < 0)$ in the interior of the $y \to +\infty$ $(y \to -\infty)$ basin by a vertical line of length $|\Delta|$ connecting the two points.] In contrast, for the example of Figs. 1(b) and 1(c), boundary points accessible from one basin are inaccessible from the other basin and many boundary points (in fact, in an appropriate sense, *most* boundary points) are inaccessible from the interior of either basin. This occurs due to the Cantor set of lines boundary structure shown in Fig. 1(c). In particular, we can consider a boundary line in Fig. 1(c) such that it is a limit set of other boundary lines from either side. Points on such a boundary line are inaccessible from either side. In this case the chosen line segment is sandwiched between an infinite set of ever thinner black and blank basin stripes accumulating on it from both sides [3]. Furthermore, as the basin stripes become thinner, they also become longer (folding back and forth) and their lengths approach infinity.

B. Outline

In this paper we give examples of basin boundaries that are simultaneously of type *c* and of either type *a* or *b*, at different points on the boundary. We also discuss the transition, with system parameter variation, between this mixed boundary type and other boundary types. In Sec. II we discuss the possibility of mixed type *c* and type *a* boundaries. We characterize these boundaries by use of the Hölder exponent [11]. It is shown that a type of continuous fractal curve $y = \tilde{f}(x)$ results whose dimension is greater than one, although the function $\tilde{f}(x)$ is differentiable at all points *x* except for a set of zero Lebesgue measure where the Hölder exponent is less than one. In Sec. III we consider bifurcations whereby the structure of the basin boundary changes as system parameters are varied. In Sec. IV we give a map example of a mixed type *c*–type *b* boundary and then compare with our previously observed boundary structure found in a four-dimensional flow [7].

II. A CONTINUOUS CURVE BASIN BOUNDARY THAT IS DIFFERENTIABLE AT ALMOST EVERY POINT BUT HAS A NONTRIVIAL FRACTAL DIMENSION

A. Hölder exponent

One way to derive the dimension formula (4) for the basin boundary of the map given by Eqs. (2a) and (2b) is by consideration of the Hölder exponent. We define the Hölder exponent $H(x)$ of a function $y = f(x)$ at the point *x* by

$$H(x) = \lim_{\Delta x \to 0} \inf\{[\ln|f(x+\Delta x) - f(x)|]/\ln|\Delta x|\} \quad (5a)$$

if the right-hand side is less than 1, and $H(x)=1$ if the right-hand side is greater than 1. More informally we write

$$\Delta y \sim |\Delta x|^H, \tag{5b}$$

where $\Delta y = |f(x+\Delta x)-f(x)|$. If $H(x)>0$, then f is continuous at x, and f is not differentiable at x for $H(x)<1$. If $f(x)$ is differentiable at x, then $H(x)=1$.

Now consider two points on the basin boundary (x_0,y_0) and $(x_0+\Delta x_0, y_0+\Delta y_0)$, where Δx_0 and Δy_0 are small, and iterate them forward n steps using Eqs. 2(a) and 2(b). They move to a pair of new points, which we denote (x_n,y_n) and $(x_n+\Delta x_n, y_n+\Delta y_n)$, both of which are necessarily also on the basin boundary. Taking n large but not too large, we may still consider Δx_n and Δy_n to be small. Since the Hölder exponent is the same at (x_0,y_0) and (x_n,y_n) (we show this later), we have

$$\Delta y_0 \sim |\Delta x_0|^H, \quad \Delta y_n \sim |\Delta x_n|^H. \tag{6}$$

The two Lyapunov exponents for the map (2a) and (2b) are $h_1=\ln \lambda_x$ and $h_2=\ln \lambda_y$. Thus mapping Δx_0 and Δy_0 forward n steps, if $H<1$ (implying $|\Delta y| \gg |\Delta x|$), we have from (2a) and (2b) that

$$\Delta x_n \sim \exp(nh_1)\Delta x_0, \quad \Delta y_n \sim \exp(nh_2)\Delta y_0. \tag{7}$$

Combining Eqs. (6) and (7) we obtain

$$H = h_2/h_1 \quad \text{for} \quad h_1 > h_2. \tag{8}$$

For $h_1<h_2$ the curve is differentiable ($H=1$). The box-counting dimension d of a curve on which the Hölder exponent is H is given by [12]

$$d = 2-H, \tag{9}$$

which with Eq. (8) yields Eq. (4). Equation (9) results from the following simple argument. Consider an ϵ grid in x-y space. For any ϵ interval $(x,x+\epsilon)$, the number of boxes from the grid necessary to vertically cover the segment of the curve $y=f(x)$ in that x interval is of order $|f(x)-f(x+\epsilon)|/\epsilon \sim \epsilon^H/\epsilon$ and the number of ϵ intervals needed to cover a finite range of x scales like $1/\epsilon$. Thus the number of ϵ boxes needed to cover the curve scales like $1/\epsilon^{2-H}$, which gives Eq. (9).

We now modify the map given by Eqs. (2a) and (2b). In particular, we replace Eq. (2b) by the logistic map [13]

$$x_{n+1} = r x_n (1-x_n). \tag{2b$'$}$$

Choosing r and λ_y such that a typical orbit for Eq. (2b$'$) is chaotic with Lyapunov exponent $\overline{h_1} > h_2 = \ln \lambda_y$, we obtain the fractal nowhere differentiable curve shown in Fig. 2(a) ($r=3.79$ and $\lambda_y=1.20$). The nowhere differentiability and fractality follows from $\overline{h_1} > h_2$ and Eqs. (8) and (9). Thus the boundary curve in Fig. 2(a) may be regarded as being similar to the one shown in Fig. 1(d) for Eqs. (2a) and (2b). [Here $\overline{h_1}$ denotes the value of the logistic map Lyapunov exponent that results for almost every choice of initial condition x in $0<x<1$. That is, if an initial condition is chosen with uniform probability density in $0<x<1$, then with probability one the result is $h_1(x)=\overline{h_1}$. Note, however, that as discussed subsequently, there are ''zero probability'' initial conditions for which $h_1(x) \neq \overline{h_1}$.]

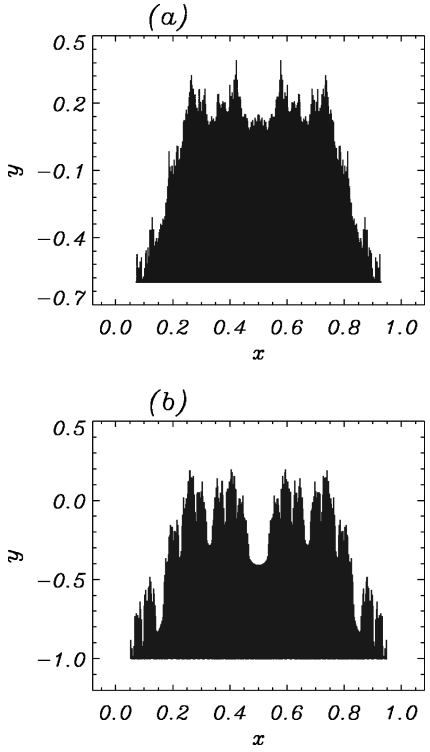

FIG. 2. Basins of attraction for the map given by Eqs. (2a) and (2b$'$) for $\lambda_y=1.20$ with (a) $r=3.79$ and (b) $r=3.835$.

Now change r so that it yields a period-3 attractor in the period-3 window. In this case almost every initial condition for Eq. (2b$'$) goes to the period-3 attractor. Hence, $h_1<0$ for almost every x so that $h_2=\ln \lambda_y > h_1$ and $H=1$, implying that the curve is differentiable at almost every point x. Note, however, that there is still a zero Lebesgue measure set of points for which the orbits of the logistic map are chaotic (but not attracting [14]). For these exceptional initial points $h_1>0$ and possibly we may also have $h_1>h_2$. The consequence of this is shown in the example illustrated in Fig. 2(b) for $r=3.835$ and $\lambda_y=1.20$. We see that the curve separating the $y=+\infty$ basin (blank) from the $y=-\infty$ basin (black) is smooth in many intervals, but that there are also many points where the boundary appears to have a nondifferentiable spike. This is a consequence of the repelling chaotic set and on the basis of Eq. (8) we claim that those points at which spikes ($H<1$) appear correspond to x values on the repelling chaotic set with $h_1(x)>h_2$.

B. Fractal dimension

One interesting aspect of this type of basin boundary structure [Fig. 2(b)] is that the basin boundary may have a fractal dimension exceeding 1, even though it is continuous everywhere and is also differentiable at all points except for a set of x of zero Lebesgue measure. To see this, we start by considering the following hypothetical case. Suppose that (i) there is a set of x points S of zero Lebesgue measure and fractal dimension $0<d_x<1$ on which the Hölder exponent has the same value for all $x \in S$ and $0<H<1$ and (ii) the

boundary is smooth at all other x points ($H=1$). Again consider an ϵ grid in x-y space. The number of ϵ boxes needed to cover the smooth portion of the curve scales as $1/\epsilon$. The contribution from the number of boxes needed to cover the nondifferentiable part of the curve scales like $(1/\epsilon^{d_x})(\epsilon^H/\epsilon)$, where the first factor is the number of ϵ intervals in x containing nondifferentiable points and the second factor is the number of boxes needed to vertically cover that part of the boundary curve lying in such an ϵ interval in x. Thus we obtain the following result for the box-counting dimension of the curve:

$$d=\begin{cases}1+d_x-H & \text{if } d_x>H\\ 1 & \text{if } d_x\leqslant H.\end{cases} \tag{10}$$

In the above argument we have assumed that the Hölder exponent H is the same for all points x in S and that $H=1$ (differentiable) everywhere else. For our basin boundary example [Fig. 2(b)] this is not the case. In particular, the one-dimensional map (2b′) has many ergodic invariant measures embedded in the set of points that do not go to the period-3 orbit. For example, there are an infinite number of unstable periodic orbits embedded in the repelling chaotic invariant set and these, in general, have different Lyapunov exponents h_1 from each other. As a result of Eq. (8) they also have different Hölder exponents if $h_1>h_2$. Nevertheless, there is an important uniformity property of the Hölder exponents: *For any ergodic invariant measure μ there is a unique constant Hölder exponent value such that the set of x values for which H(x) takes on this value has μ measure 1* [15].

To see that this must be so we first note that, by the smoothness of the map, one iterate of the map applied to a small region of the boundary curve results in an approximate linear deformation of the small region. Thus by Eq. (5a), H at a point and at its iterate are the same. Now assume that the italicized statement above is not true. Then there is a number H_* such that we can define two sets of x values S_1 and S_2 for which $\mu(S_1)>0$ and $\mu(S_2)>0$ with $H(x)\geqslant H_*$ for all x in S_1 and $H(x)<H_*$ for all x in S_2. Since H is invariant to one application of the map, no iterate of a point in S_1 can map to S_2 and vice versa. This contradicts the ergodicity of μ, thus proving that H must be the same for a set of x values of μ measure 1. Note that, by Oseledec's multiplicative ergodic theorem, the Lyapunov exponents are also the same for almost every point with respect to an ergodic measure μ. [Thus, for any ergodic invariant measure, the two sides of Eq. (8) are constant for almost all x with respect to μ, $H=h_2/h_1$.]

With this knowledge we can now make a modification of Eq. (10) that we conjecture applies to cases such as our example in Fig. 2(b),

$$d=\begin{cases}1+\chi_{max} & \text{if } \chi_{max}>0\\ 1 & \text{if } \chi_{max}\leqslant 0,\end{cases} \tag{11a}$$

where

$$\chi_{max}=\lim_{\mu}\sup[\tilde{d}_x(\mu)-h_2/\tilde{h}_1(\mu)] \tag{11b}$$

is the maximum value over all ergodic invariant measures μ for the map (2b′) of the dimension $\tilde{d}_x(\mu)$ of μ minus the Hölder exponent of the measure μ [the Hölder exponent uniform on the measure μ is by Eq. (8) equal to $h_2/\tilde{h}_1(\mu)$, with $\tilde{h}_1(\mu)$ the Lyapunov exponent for the measure μ]. Equation (11) is motivated by the observation that the dimension of the union of a finite (countable infinite) number of sets is equal (at least equal) to that of the set whose dimension is largest. In particular, if we evaluate $\chi(\mu)\equiv\tilde{d}_x(\mu)-h_2/\tilde{h}_1(\mu)$ for *any* invariant measure [not necessarily the measure that maximizes $\chi(\mu)$], then application of Eq. (10) with this value inserted for d_x-H yields a lower bound for d,

$$d\geqslant\tilde{d}(\mu)\equiv\begin{cases}1+\chi(\mu) & \text{if } \chi(\mu)>0\\ 1 & \text{if } \chi(\mu)\leqslant 0.\end{cases} \tag{12}$$

Furthermore, if $\chi(\mu)$ is positive for any μ, then Eq. (12) provides a sufficient condition for the box-counting dimension of the basin boundary curve to be greater than one. In practice, in a numerical example, such as that of Fig. 2(b), we have no way of performing the maximization prescribed by Eq. (11b). (For a special example that is analytically solvable see the Appendix.) Thus, in general, the only numerical results accessible to us will be by use of a particular measure and Eq. (12). In this regard we shall be utilizing the ''natural'' measure on the repelling invariant chaotic set of the one-dimensional map (2b′). We denote this measure μ_*.

In addition to Eq. (12), there is a second useful result obtainable from Eq. (11). Specifically, the border separating the case $d>1$ from the case $d=1$ (i.e., $\chi_{max}=0$) gives a condition on h_2. This condition can be determined by noting that the dimension $\tilde{d}_x(\mu)$ of a measure of a one-dimensional map is [16]

$$\tilde{d}_x(\mu)=\frac{\tilde{h}_{met}(\mu)}{\tilde{h}_1(\mu)}, \tag{13}$$

where $\tilde{h}_{met}(\mu)$ is the metric entropy for μ. The condition $\chi_{max}=0$ then gives [see Eq. 11(b)] $h_2=\lim_{\mu}\sup\tilde{h}_{met}(\mu)$. The right-hand side of this equation is just the topological entropy, which we denote h_{top}. Thus we obtain from Eq. (11)

$$d>1 \quad \text{for } h_2<h_{top}, \tag{14a}$$

$$d=1 \quad \text{for } h_2\geqslant h_{top}. \tag{14b}$$

We now apply Eq. (12) to the case shown in Fig. 2(b). We evaluate the lower bound $\tilde{d}(\mu_*)$ from Eq. (12). We then directly evaluate d by use of the uncertainty exponent method [1,6] and compare with the predicted lower bound.

To find $\tilde{h}_1(\mu_*)$ at $r=3.835$ [the value used for Fig. 2(b)], we sprinkle many initial conditions N randomly in the interval [0,1] and iterate each one $T\gg 1$ iterates (say $T=100$). We then determine those initial conditions whose orbits have still not yet fallen close to the period-3 orbit at iterate T (here we, somewhat arbitrarily, define an orbit as falling close to the period-3 orbit if it is ever within a distance of 0.01 of the middle point of the three points visited). Selecting those and averaging their Lyapunov exponents computed over the time

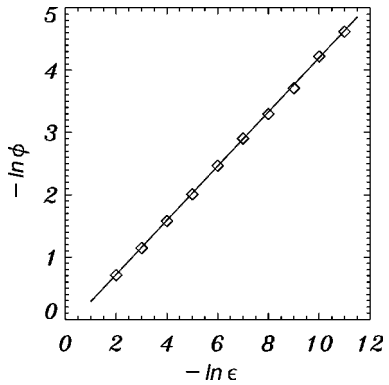

FIG. 3. $\ln \phi(\epsilon)$ versus $\ln \epsilon$.

interval 0 to $T-5$, we obtain an estimate of the Lyapunov exponent h_1 for the natural measure on the repelling invariant chaotic set. (The true value is obtained in the limit $N \to \infty$, $T \to \infty$.) In this way we obtain

$$\tilde{h}_1(\mu_*) \cong 0.498. \tag{15}$$

To obtain $\tilde{d}_x(\mu_*)$ for the case where μ is the natural measure, $\mu = \mu_*$, we note that in this case [17]

$$\tilde{h}_{met}(\mu_*) = \tilde{h}_1(\mu_*) - \frac{1}{\tau}, \tag{16a}$$

which from Eq. (13) gives

$$\tilde{d}_x(\mu_*) = \frac{\tilde{h}_1(\mu_*) - \dfrac{1}{\tau}}{\tilde{h}_1(\mu_*)}, \tag{16b}$$

where τ is the decay time of the repelling invariant chaotic set. This gives the lower bound for d,

$$\tilde{d}(\mu_*) = 2 - \frac{h_2 - \dfrac{1}{\tau}}{\tilde{h}_1(\mu_*)}. \tag{17}$$

The decay time τ is numerically obtained by sprinkling many initial conditions uniformly in $[0,1]$, iterating them, and recording the number of orbits $N(t)$ at iterate t that have still not yet fallen within some small neighborhood of the period-3 orbit. For large t, $[N(t)/N(0)] \sim \exp-(t/\tau)$. Thus to find τ we plot $\ln[N(t)/N(0)]$ versus t, fit a straight line to the resulting data, and estimate $1/\tau$ as minus the slope of this

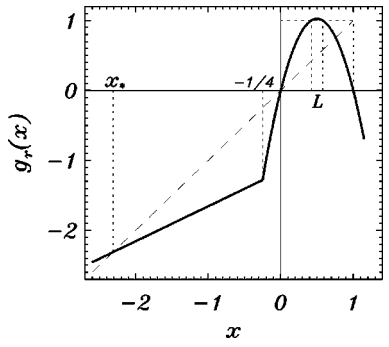

FIG. 4. Graph of $g_r(x)$ for $r = 4.1$.

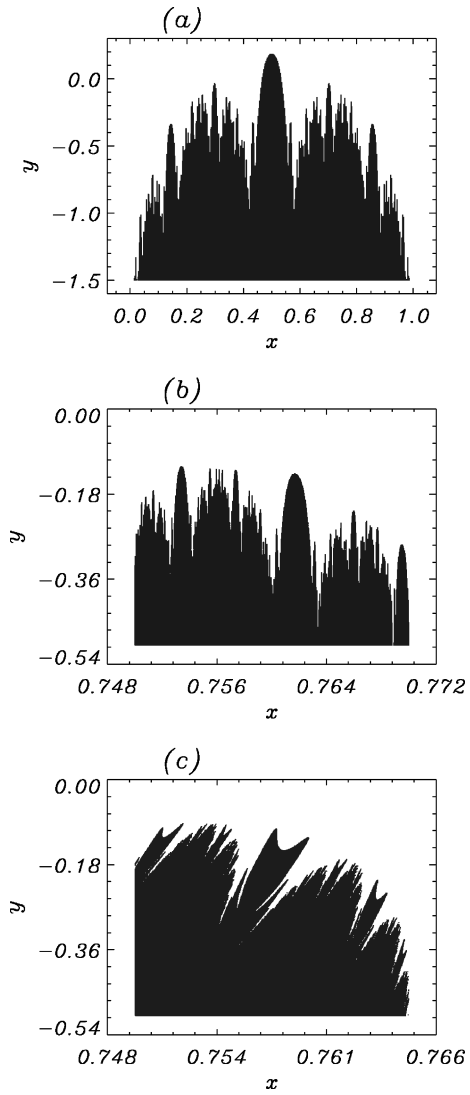

FIG. 5. (a) Basin boundary for the map given by Eqs. (2a) and (2b″). (b) Enlargement of (a). (c) Basin boundary for the map given by Eqs. (2a) and (2b‴).

line. We obtain $1/\tau = 0.041$. Using Eqs. (15) and (16b) together with $h_2 = \ln \lambda_y = \ln 1.20 = 0.182$ in Eq. (17) yields

$$\tilde{d}(\mu_*) \cong 1.55. \tag{18}$$

As previously mentioned, the direct calculation of d is done by use of the uncertainty exponent. To do this we choose some region of x-y space containing the boundary [e.g., the region shown in Fig. 2(b)]. We then sprinkle many initial conditions (x_i, y_i), $i = 1,2,\ldots,N$ with N very large, randomly in this region. Next we perturb each initial condition to a new point $(x_i + \epsilon, y_i + \epsilon)$. We then iterate each pair (x_i, y_i) and its perturbation. The fraction of original points N for which the point and its perturbation eventually go to different attractors (in the present example, to large positive y and large negative y) is denoted $\phi(\epsilon)$. For a boundary that is everywhere smooth $\phi(\epsilon)$ scales like ϵ for small ϵ. For a boundary with box-counting dimension $d > 1$, on the other hand, $\phi(\epsilon)$ scales like ϵ^α with $0 < \alpha < 1$ and $\alpha = D - d$, where D is the dimension of phase space [1,6]. (This shows the practical importance of the existence of a fractal basin boundary; if α is substantially less than one, the probability

TABLE I. Characterization of boundary types α, β, γ, and δ.

Boundary types	d	Set of x for smooth set	Nondifferentiable set	χ_{max}	H_{min}	$\overline{H}$	Figure
α	1	all x	empty	<0	1	1	7(a)
β	1	Lebesgue measure one	$1>d_x>0$	<0	<1	1	7(b)
γ	>1	Lebesgue measure one	$1>d_x>0$	>0	<1	1	2(b) 7(c)
δ	>1	empty	$d_x=1$	>0	<1	<1	2(a)

of incorrectly predicting the attractor from an initial condition with some small error in its specification is greatly enhanced.) Figure 3 shows a plot of $\ln \phi(\epsilon)$ versus $\ln \epsilon$ for the example of Fig. 2(b). The slope of a straight line fitted to this data is $\alpha \cong 0.44$, corresponding to

$$d = 2 - \alpha \equiv 1.56. \tag{19}$$

This is consistent with the lower bound estimate (18) and indeed the lower bound estimate (18) is close to the estimated d value in Eq. (19).

It is instructive to consider another example of this type of boundary. For this example we again use Eq. (2a) for the y component of the map. For the x component of the map we use

$$x_{n+1} = g_r(x_n) \equiv \begin{cases} r x_n (1 - x_n) & \text{for } x_n \geq -\dfrac{1}{4} \\ 0.5\left(x_n + \dfrac{1}{4}\right) - \dfrac{5r}{16} & \text{for } x_n < -\dfrac{1}{4}. \end{cases} \tag{2b''}$$

The map function $g_r(x)$ is continuous and is graphed in Fig. 4 for $r = 4.1$, which is the value we use below. Since $r > 4$, there is only a chaotic transient set in $0 < x < 1$; almost every initial condition in $0 < x < 1$ eventually falls into the loss region L (Fig. 4), two iterates after which it maps to negative x, and then is attracted by the fixed point $x = x_* < 0$ (Fig. 4). Thus almost all initial conditions for the one-dimensional map (2b″) go to $x = x_*$. There is, however, an invariant chaotic Cantor set in $0 \leq x \leq 1$ that remains in $0 \leq x \leq 1$ forever. Thus, as in our previous example [Fig. 2(b)], for λ_y not too large, we expect singularities ($H < 1$) on this Cantor set. Figure 5(a) shows the resulting basins for the case $\lambda_y = 1.3$ and Fig. 5(b) shows a blowup of a small region of the boundary in Fig. 5(a). Measurements of the uncertainty dimension in this case give $d \cong 1.53$. Thus the boundary of Fig. 5(a) has all the same essential features as the boundary of Fig. 2(b).

C. Typicality

We claim that basin boundaries of the character we have been discussing should occur in cases that might naturally arise in the consideration of dynamical systems in typical applications. While some evidence of this is provided by the differential equations example [7] discussed at the end of Sec. IV, we note that the examples we have discussed so far have the feature that the x dynamics is uninfluenced by the evolution of y. This is a special type of property not to be expected in typical systems encountered in practice. To verify that this special feature is not responsible for the phenomena we have demonstrated, we modify our map (2a) and (2b″) to couple the y dynamics to the x dynamics. To this end we replace Eq. (2b″) by

$$x_{n+1} = g_r(x_n) + 0.06 y_n. \tag{2b''}$$

Figure 5(c) shows a blowup of a small section of the basin boundary for the two-dimensional map given by Eqs. (2a) and (2b″) with $\lambda_y = 1.3$ and $r = 4.1$ [as in Fig. 5(a)]. Comparing Figs. 5(b) and 5(c), it is seen that they appear visually to have similar character.

One difference between the example of Fig. 5(b) and the example of Fig. 5(c) is the following. For the example of Fig. 5(b) the boundary is a function $y = f(x)$. That is, there is a rectangular coordinate system such that for each x there is one and only one boundary point, thus determining a unique value of y. For Fig. 5(c) it is not clear that such a nice coordinate system could be found and this situation is to be expected in typical cases. Thus we seek to characterize the potential common features of the example in Fig. 5(b) and cases like that in Fig. 5(c) in such a way that these characterizations are independent of coordinate system. We propose the following properties as potential coordinate-system-independent characterizations on the basis of which we say that the basin boundaries in Figs. 5(b) and 5(c) are similar.

(i) All boundary points are accessible from both basins. (As discussed in Sec. I A, this is not the case for type (b) basins [e.g., Figs. 1(b) and 1(c)].)

(ii) The boundary is smooth at all points except for a totally disconnected set of nonsmooth points (i.e., it is not possible to connect any two points in the nonsmooth set by a curve completely contained in the nonsmooth set). Furthermore, any neighborhood of a point where the boundary is not smooth contains smooth pieces. [We have verified the latter for Fig. 5(c) by making successive blowups around one of the nonsmooth points.]

(iii) The boundary (although nonsmooth only on a set of points of box-counting dimension less than one) has a box-counting dimension greater than one. [Using the uncertainty exponent method we have estimated that the dimension of the basin boundary in Fig. 5(c) is $d \cong 1.48$.]

III. CHANGES IN BASIN BOUNDARY STRUCTURE WITH VARIATION OF SYSTEM PARAMETERS

The types of basin boundaries shown in Fig. 2(a) (a nowhere differentiable curve with dimension $d > 1$) and in Fig. 2(b) (an almost everywhere differentiable curve with $d > 1$) are not the only possible basin boundary types for the map given by Eqs. (2a) and (2b′). In fact, based on the discussion in Sec. II [particularly Eqs. (8)–(14)], we can distinguish

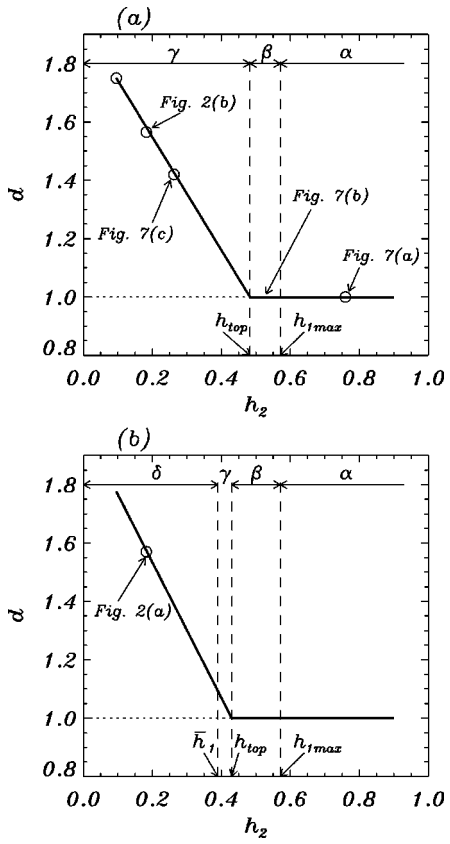

FIG. 6. Graph of d versus h_2 for (a) $r=3.835$ and (b) $r=3.79$. The values of $\overline{h}_1$ and h_{top} in 6(b) are estimated from the graph of these quantities versus r in Ref. [21].

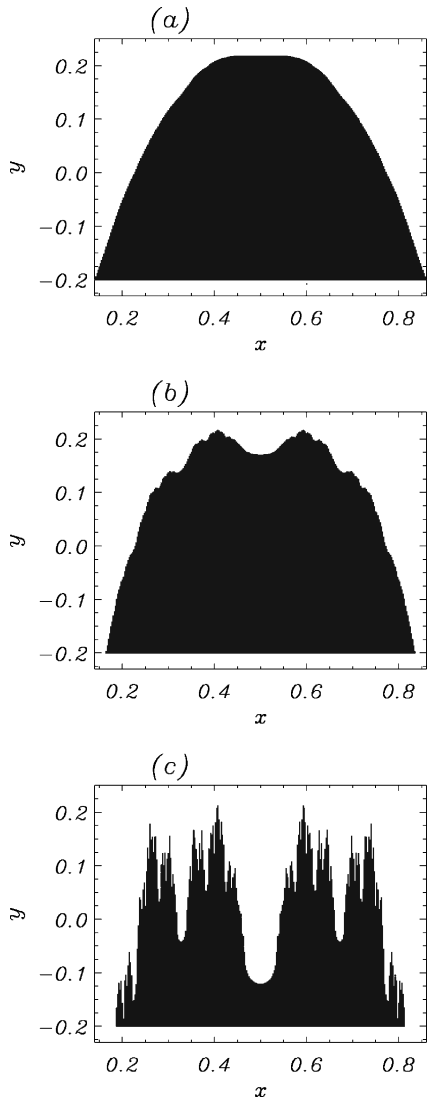

FIG. 7. Graph of basin boundary pictures for (a) $r=3.835$ and $\lambda_y=2.1$, (b) $r=3.835$ and $\lambda_y=1.7$, and (c) $r=3.835$ and $\lambda_y=1.3$.

four boundary types depending on the map parameters. We label these boundary types α, β, γ, and δ, in order of increasing fractality: *type* α, everywhere smooth curve ($d=1$); *type* β, smooth almost everywhere with singularities [$H(x)<1$] on a fractal set of x and a curve dimension $d=1$; *type* γ, same as β, but $d>1$; and *type* δ, Weierstrass curve (i.e., nowhere differentiable and $d>1$).

The boundaries in Figs. 2(a) and 2(b) are of types δ and γ, respectively. Table I provides further characterization of the above boundary types. In Table I, H_{min} denotes the smallest Hölder exponent at any point on the boundary curve, which, from Eq. (8), is

$$H_{min}=\frac{h_2}{h_{1_{max}}} \tag{20}$$

if the right-hand side of Eq. (20) is less than 1, and $H_{min}=1$ otherwise. In Eq. (20), $h_{1_{max}}$ denotes the logistic map Lyapunov exponent maximized over all invariant measures [18]. Also, $\overline{H}$ in Table I is the Hölder exponent assumed for initial x at almost every point in $0\leqslant x\leqslant 1$, which from Eq. (8) is

$$\overline{H}=\frac{h_2}{\overline{h}_1} \tag{21}$$

if the right-hand side of Eq. (21) is a positive number less than 1, and $\overline{H}=1$ otherwise. The quantity $\overline{h}_1$ is the logistic map Lyapunov exponent for Eq. (2b″) assumed for almost every initial condition in $0\leqslant x\leqslant 1$ (i.e., if an initial x value is chosen randomly, with probability 1, the resulting Lyapunov exponent is $\overline{h}_1$).

In order to see how these different boundary types arise, consider Fig. 6(a), which schematically shows the dimension of the basin boundary d (some points numerically determined by the uncertainty exponent technique are shown as solid dots in the figure [19]) as a function of $h_2=\ln\lambda_y$ for $r=3.835$. This r value is that used for Fig. 2(b) and yields a period-3 attractor for the logistic map. Consequently, $\overline{h}_1<0$ (this will imply that a type δ boundary does not occur for this case). Also shown in Fig. 6(a) as vertical dashed lines are ranges where boundaries of types α, β, and γ occur. In region α, h_2 exceeds the Lyapunov exponent of the logistic map for *all* initial conditions in x, $h_2>h_{1_{max}}$. Thus, by Eq. (8), $H=1$ everywhere and the curve is smooth. An example of this is shown in Fig. 7(a).

As h_2 is decreased, there comes a point where it passes through the largest possible Lyapunov exponent $h_{1_{max}}$. For

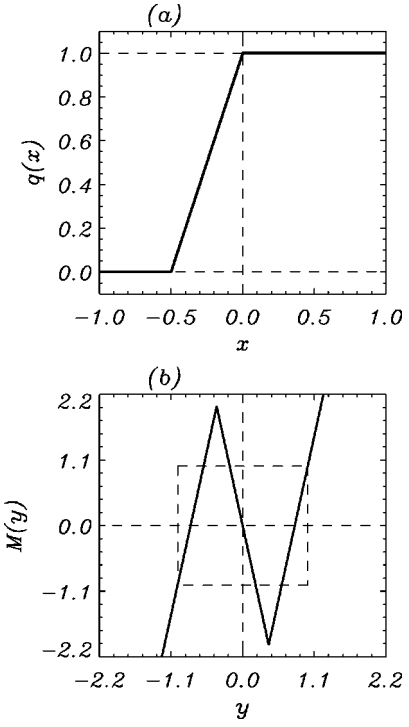

FIG. 8. (a) $q(x)$ versus x. (b) $M(y)$ versus y.

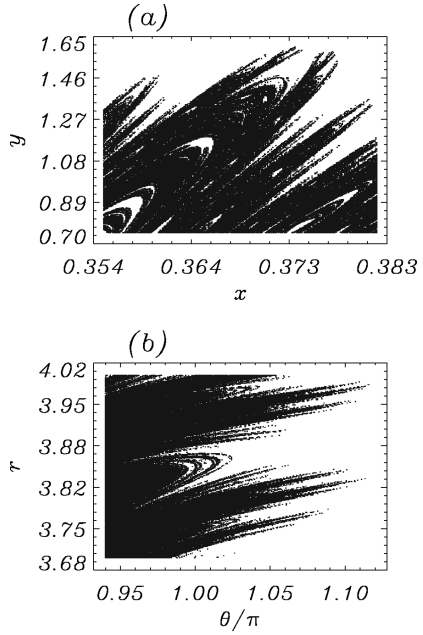

FIG. 9. (a) Basins of attraction for $y \to +\infty$ (blank) and $y \to -\infty$ (black) for the map given by Eqs. (2b‴) and (2a′). (b) Basins of attraction (Fig. 6 of Ref. [7]).

$h_2 < h_{1_{max}}$ there is a set of x points where $H(x) < 1$ and the boundary curve is nondifferentiable (singular) at these points. When this first occurs, χ_{max} is still negative and so $d = 1$. In fact, it is expected that $h_{1_{max}}$ is attained for a low-period unstable periodic orbit [18]. In this case, the applicable measure is the δ measure on the periodic orbit and $d_x(\mu) = 0$ for this μ. Consequently, at $h_2 = h_{1_{max}}$, we have $\chi_{max} = -h_2/h_{1_{max}} < 0$.

We have not determined the precise point $h_2 = h_{1_{max}}$ corresponding to the border between α and β in Fig. 6(a). Visual inspection of basin boundaries for different h_2 values suggests the approximate location of this border shown in Fig. 6(a). The ''visual'' determination of the border between regions α and β is consistent with $h_{1_{max}}$ being the Lyapunov exponent of the period-2 unstable periodic orbit embedded in the chaotic set, $h_{1_{max}} = 0.571$ (see[18]). We also note that there is an unstable period-1 orbit at $x = 0$ that has a still larger Lyapunov exponent $h_1(x = 0) = \ln r$ than the period-2 orbit. The period-1 orbit, however, is isolated and not in the chaotic set. Thus, while it can lead to a singularity [$H(x = 0) < 1$], this singularity is isolated and for that reason we choose to exclude it from our consideration in the definition of the border between regions α and β. That is, we effectively restrict our attention to the part of the boundary lying in region $\eta < x \leqslant 1$ where η is a small positive number. (In this region, aside from the period-3 attractor, all invariant sets are contained within an invariant fractal Cantor set and this set has a dense orbit.)

As h_2 is reduced past $h_2 = h_{1_{max}}$, the box-counting dimension of the set of x values where $H(x) < 1$ grows from its value of zero at $h_2 = h_{1_{max}}$. Thus there is a range (region β) where $\chi_{max} < 0$ and $H(x) < 1$ on a Cantor set. In this case, because $\chi_{max} < 0$, the curve dimension d is still one [Eq. (11)]. An example of such a boundary is shown in Fig. 7(b).

A further decrease of h_2 eventually results in $\chi_{max} > 0$ as the border between region β and region γ is crossed. By Eq. (14) this occurs at $h_2 = h_{top}$. The topological entropy in a window of the logistic map is constant (i.e., independent of r for r in the window) and may be computed analytically from consideration of the symbolic dynamics associated with the given window. In the case of the period-3 window, the topological entropy is the logarithm of the golden mean $h_{top} = \ln[(1+\sqrt{5})/2] = 0.483$ and region γ corresponds to $h_2 < 0.483$. Examples of basin boundaries in region γ are shown in Figs. 7(c) and 2(b). Corresponding to its lower dimension [see Fig. 6(a)], the boundary in Fig. 7(c) visually appears less wiggly than that in Fig. 2(b) [note the expanded vertical scale in Fig. 7(c)].

Figure 6(b) shows d versus $h_2 = \ln \lambda_y$ for the r value for Fig. 2(a) [20], namely, $r = 3.79$. At this r value the logistic map has a chaotic attractor with $\overline{h_1} > 0$. In this case, if $h_2 < \overline{h_1}$, then $H(x) < 1$ for almost all x and the basin boundary curve is everywhere nondifferentiable [i.e., it is of type δ as in Fig. 2(a)]. As h_2 is increased from $h_2 < \overline{h_1}$ to $h_2 > \overline{h_1}$, the Hölder exponent $H(x)$ becomes 1 for all but a zero Lebesgue measure fractal set of x values and we obtain a basin boundary of type γ.

Finally, we note that other parameter variations can be discussed in a similar vein. For example, fixing h_2 at the value for Fig. 2(a) and increasing r, the value of $\overline{h_1}$ varies in an erratic manner as small windows of high-period orbits are traversed. Such small windows probably occupy a small fraction of the Lebesgue measure between $r = 3.79$ and the r value at the beginning of the period-3 window. In many experimental settings parameter values are not continuously varied but are changed in small finite steps. In such cases, it

may be unlikely that a small window is encountered, and thus they may not be relevant in many experimental settings. If we ignore them and concentrate on the upper envelope of the $\overline{h_1}$ versus r curve, then, as the beginning of the period-3 window is approached, $\overline{h_1} \to 0$. Thus, in this envelope sense, we expect to see a transition from a type δ boundary [Fig. 2(a)] to a type γ boundary with increasing r. We note that this transition occurs in the region of chaotic attractors for the logistic map at an r value *below* that at the beginning of the period-3 window.

IV. MIXED TYPE *b*–TYPE *c* BASIN BOUNDARIES

To obtain a boundary mixing type b characteristics with type c characteristics, we aim to make the dynamics on the boundary similar to that of the map (2a) with (2b′) in some region of the boundary, while in some other region we aim to make it similar to the dynamics yielding the boundary in Fig. 1(b). For this purpose we consider the two-dimensional map given by Eq. (2b‴) and

$$y_{n+1} = q(x_n)[\lambda_y y_n + \cos(2\pi x_n)] + [1 - q(x_n)]M(y_n), \tag{2a′}$$

where $q(x)$ and $M(y)$ are the continuous piecewise linear functions shown in Figs. 8(a) and 8(b).

The quantity $q(x)$ makes a continuous transition from $q(x) \equiv 1$ in $x > 0$ to $q(x) \equiv 0$ in $x < -1/2$. Thus, in $x > 0$ we have

$$y_{n+1} = \lambda_y y_n + \cos(2\pi x_n),$$

$$x_{n+1} = 4.1 x_n (1 - x_n) + 0.06 y_n .$$

For orbits that remain in $x > 0$ this dynamics is similar to that for Eqs. (2a) and (2b‴), which yielded Fig. 5(c). Furthermore, in the case of Fig. 5(c) the set corresponding to the nondifferentiable peaks has an orbit visiting these peaks and this orbit stays in $x > 0$. Thus our map (2b‴) and (2a′) should have similar peaks.

For $x < 1/2$, Eqs. (2b‴) and (2a′) reduce to

$$y_{n+1} = M(y_n),$$

$$x_{n+1} = 0.5 x_n + 0.06 y_n - 0.644.$$

This map yields a boundary consisting of a Cantor set of strips corresponding to the $y \to +\infty$ basin and the $y \to -\infty$ basin[22]. Furthermore, we expect that almost all points in $x > 0$ eventually fall in $x < 0$ (because $r > 4$). Thus the Cantor set of stripes structure should be dense in the boundary, even for $x > 0$.

Figure 9(a) shows a section (in $x > 0$) of the basin of attraction plot for the map given by Eqs. (2b‴) and (2a′) with $\lambda_y = 1.03$. The boundary appears to consist of a mixture of parts with sharp peaks plus other parts with locally black and blank striped regions. Figure 9(b) shows a basin of attraction plot obtained for a system of differential equations [7] used to study the problem of phase synchronization of chaos. We believe that these two plots evidence the same qualitative character, namely, a fractal set of sharp peaks with striated basin strips similar to those of Figs. 1(b) and 1(c) densely intertwined.

ACKNOWLEDGMENTS

We thank B. R. Hunt for useful discussion. This work was supported by the U. S. Department of Energy (High Performance Computing and Communications Program), by the CNPq-NSF (Division of International Programs), and by the Office of Naval Research (Physics).

APPENDIX: ANALYTICAL EXAMPLE FOR χ_{max}

In Eq. (11) we require the value of $\chi(\mu)$ maximized over all ergodic invariant measures of the one-dimensional map. We also commented following Eq. (11) that in practice it is not possible to carry out this maximization. While this statement is true in general, in this appendix, as an illustration, we consider a special example for which the maximization can be done. In particular, we consider the two-dimensional map given by Eq. (2a) together with the one-dimensional map

$$x_{n+1} = \begin{cases} \alpha^{-1} x_n & \text{for } 0 \leq x < \alpha \\ \beta^{-1}(x_n - \alpha) & \text{for } \alpha \leq x \leq 1, \end{cases} \tag{A1}$$

where $\beta = 1 - \alpha$. This map may be viewed as a discontinuous map on the x interval $0 \leq x \leq 1$ (discontinuity at $x = \alpha$) or as a continuous map on the circle (where x measures the distance around the circumference of the circle and the length of the circumference is 1). For an ergodic invariant measure of the one-dimensional map (A1), there will be some fraction of the time that an orbit generating this measure spends in $(0,\alpha)$, call it p, and a fraction $1-p$ that it spends in $(\alpha,1)$. In this case we have $\tilde{h}_1(\mu) = p \ln(1/\alpha) + (1-p)\ln(1/\beta)$. Considering all μ's with the same fraction p for $(0,\alpha)$, the maximum randomness of an orbit [yielding the maximum $\tilde{h}_{met}(\mu)$] comes when visits to $(0,\alpha)$ and $(\alpha,1)$ are uncorrelated. That is, the measure is generated by the random process that says that, on any given iterate, the orbit is in $(0,\alpha)$ with probability p and in $(\alpha,1)$ with probability $1-p$, independent of which of these intervals were visited in all previous history. The metric entropy is then given by the Shannon information for the uncorrelated events $\tilde{h}_{met} = p \ln(1/p) + (1-p)\ln[1/(1-p)]$. Thus we can assign a maximum value of $\chi(\mu)$ over all measures μ with a given p $(0 \leq p \leq 1)$. We denote this $\chi(p)$,

$$\chi(p) = \frac{p \ln \frac{1}{p} + (1-p)\ln \frac{1}{1-p} - h_2}{p \ln \frac{1}{\alpha} + (1-p)\ln \frac{1}{\beta}}.$$

χ_{max} is then the maximum over p of the quantity $\chi(p)$.

[1] S. W. McDonald, C. Grebogi, E. Ott, and J. A. Yorke, Physica D **17**, 125 (1985).

[2] C. Grebogi, E. Ott, and J. A. Yorke, Phys. Rev. Lett. **50**, 935 (1983); Ergodic Theory Dyn. Syst. **5**, 341 (1985); E. Ott, *Chaos in Dynamical Systems*, (Ref. [6]) pp. 163–164. **(**For the two-dimensional map given by Eq. (2a) and $x_{n+1}=M(x_n)$, where M is a general one-dimensional map, the analysis of Grebogi *et al.* yields that the basin boundary can be represented analytically by the convergent series $y=-\Sigma_{j=1}^{\infty}\lambda_y^{-j}\cos[2\pi M^{j-1}(x)]$, where $M^j(x_n)=x_{n+j}$. We shall, however, not need to utilize this representation in the present paper.**)**

[3] C. Grebogi, E. Ott, and J. A. Yorke, Phys. Rev. Lett. **56**, 1011 (1986); Physica D **24**, 243 (1987).

[4] C. Grebogi, S. W. McDonald, E. Ott, and J. A. Yorke, Phys. Lett. **99A**, 415 (1983).

[5] C. Grebogi, E. Kostelich, E. Ott, and J. A. Yorke, Physica D **25**, 347 (1987).

[6] E. Ott, *Chaos in Dynamical Systems* (Cambridge University Press, Cambridge, 1993), pp. 152–166.

[7] E. Rosa, Jr., E. Ott, and M. H. Hess, Phys. Rev. Lett. **80**, 1642 (1998).

[8] In this paper we restrict consideration to *typical* dynamical systems, i.e., systems whose behavior is not due to special delicately chosen properties (e.g., symmetries). For example, in addition to the three basin types *a*, *b*, and *c*, another type of basin boundary that exists for systems with the special property of having an invariant submanifold is the riddled basin. Riddled basins in situations with invariant submanifolds are of interest in chaos synchronization or else arise naturally for systems with a symmetry. See, e.g., J. C. Alexander, J. A. Yorke, Z. You, and I. Kan, Int. J. Bifurcation Chaos Appl. Sci. Eng. **2**, 795 (1992); E. Ott *et al.*, Physica D **76**, 384 (1994).

[9] As A increases past the value $A=A_1\equiv-(J+1)^2/4$, a saddle-node bifurcation creates two fixed points (one attracting, the other a saddle). For $A<A_1$, the only attractor is ∞. For A slightly larger than A_1 there are two attractors, one at $(|x|,|y|)=\infty$ and the other an attracting fixed point. For $A=1.150$ the basin boundary is the stable manifold of the period-1 saddle (created at $A=A_1$), apparently a smooth curve. This smooth curve becomes fractal as A is varied from 1.150 to 1.395 following a homoclinic tangency of the period-1 saddle, characterizing a *smooth-fractal basin boundary metamorphosis*. For more details see Ref. [3].

[10] In Ref. [5], the system studied has boundary types *a* and *b* mixed on an arbitrarily fine scale. In particular, for any region where the boundary is fractal, one can find within that region a subregion where the boundary is smooth. Thus smooth pieces of the boundary are said to be *intertwined* with type *b* fractal parts of the boundary.

[11] A similar approach has been previously used by B. R. Hunt, E. Ott, and J. A. Yorke, [Phys. Rev. E **55**, 4029 (1997)] in the context of generalized synchronism of chaos. Indeed, the situation we consider in Sec. II has similarities to a case of an attractor considered in Sec. III of the paper of Hunt *et al.*

[12] See, e.g., J. Feder, *Fractals* (Plenum, New York, 1988), p. 186.

[13] Note that the two-dimensional noninvertible map examples (2a) with (2b) or (2a) with (2b′) can also be thought of as representing three-dimensional invertible map systems. For example, we can append to the x and y dynamics an additional z dynamics given by $z_{n+1}=\lambda_z z_n+u(x_n-1/2)$, where $u(x)$ is the unit step function and $0<\lambda_z<1/2$, $0\leqslant z_n\leqslant 2$. In this case, given z_{n+1}, we have that $x_n<1/2$ if $z_{n+1}<1$ and $x_n\geqslant 1/2$ if $z_{n+1}\geqslant 1$. This information then allows one to obtain x_n and z_n given x_{n+1} and z_{n+1}. Thus the three-dimensional map is invertible. The basin boundary is still of the form $y=f(x)$ (i.e., it is independent of z), so that all of the analysis for the two-dimensional noninvertible case still applies.

[14] Points exactly on the repelling chaotic set stay there forever, never going to the period-3 attractor. Points initialized very near the repelling chaotic set experience a chaotic transient [1,6] whereby they closely follow a chaotic orbit on the repelling chaotic set, but after some time move away from it and asymptotically approach the period-3 attractor.

[15] Alternatively, we say that $H(x)$ takes on the same value except for x in a set whose μ measure is zero. The meaning of the phrase ''except for a set whose μ measure is zero'' may be clarified by an example. In particular, for an unstable period-p orbit, the ergodic invariant measure μ is $1/p$ multiplied by the sum of p delta functions on the p elements of the periodic orbit. The Hölder exponent is the same at each of these p points. The set of points with different H has μ-measure zero for this δ-function measure because this set does not include any of the p points on the periodic orbit.

[16] L.-S. Young, Ergodic Theory Dyn. Syst. **2**, 108 (1982).

[17] H. Kantz and P. Grassberger, Physica D **17**, 75 (1985).

[18] It has been conjectured that, for typical cases, quantities such as h_1 assume their maximum (or minimum) values on low period periodic orbits. [B. R. Hunt and E. Ott, Phys. Rev. E **54**, 328 (1996).]

[19] In Fig. 6 we do not show points for d computed near $h_2=h_{top}$ because we believe that the computation is inaccurate there. Indeed an analytical argument predicts that the number of ϵ boxes needed to cover the curve scales like $\epsilon^{-1}[\ln(1/\epsilon)]^{1/2}$ at $h_2=h_{top}$. Because of the presence of the logarithmic term d would be overestimated unless very small ϵ values were considered. This is not possible with current computer resources.

[20] In all of the above [particularly Figs. 6(a) and 6(b)] $h_2=\ln\lambda_y$ is varied independently of the x dynamics. In a more general case [e.g., $\lambda_y\rightarrow\lambda_y(x)$ in Eq. (2a)] h_2 might also depend on the measure μ of the x dynamics. In such a case the basic ideas of the previous discussion still apply with minor modification. [For example, replace h_2 in Eq. (11b) by $\tilde{h}_2(\mu)$, the y Lyapunov exponent for the logistic map measure μ.]

[21] D. Ruelle, *Chaotic Evolution and Strange Attractors* (Cambridge University Press, Cambridge, 1989), p. 60.

[22] For example, for a discussion directly applicable to the map $y_{n+1}=M(y_n)$ of Fig. 8(b) see pp. 156 and 157 of Ref. [6].